

Research Article

Reda EL-Mernissi*, Marwa Alaqrbeh, Ayoub Khaldan, Mohammed Kara*, Omkulthom Al kamaly, Anwar M. Alnakhli, Tahar Lakhli, Abdelouahid Sbai, Mohammed Aziz Ajana, Mohammed Bouachrine

3D-QSAR, molecular docking, ADMET, simulation dynamic, and retrosynthesis studies on new styrylquinolines derivatives against breast cancer

<https://doi.org/10.1515/chem-2024-0041>

received March 13, 2024; accepted May 6, 2024

Abstract: Breast cancer is the most common illness among women, accounting for 25% of all diagnoses, as stated by the American Cancer Society. Current research focuses on

43 compounds of styrylquinoline derivatives as potential inhibitors of tubulin to design a new drug that could potentially be effective against breast cancer cells in humans. The target compounds were subjected to a three-dimensional quantitative structure-activity relationship/comparative molecular similarity indices analysis (CoMSIA) approach, where CoMSIA models were used; the best results obtained are ($Q^2 = 0.84$, $R^2 = 0.97$, $r_{\text{ext}}^2 = 0.91$), H-bond acceptor field was discovered to be important for increasing inhibitory activity by examining the contour maps (54%), and it plays a key role in the prediction of anticancer activity. Based on the contour maps of the CoMSIA models, we obtained information that allows us to propose four new molecules with higher cancer inhibitory than the 43 compounds found in the literature. The molecular docking was applied to determine the likely types of binding between the tubulin protein (PDB ID: 4O2B) and the proposed compounds, and the results show that M1 has a higher total score of 6.53 and two interactions with important conventional hydrogen bond type, followed by compound M2 with a total score of 5.74. Furthermore, the designed molecules showed better pharmacokinetic properties based on absorption, distribution, metabolism, excretion, and toxicity properties. Molecular dynamics simulations at 100 ns were conducted to confirm the binding stability of the selected ligands (M1 and M2) with tubulin protein. The simulation parameters used in the current study are root mean square deviation, root mean square fluctuation, H-bond, Rg, solvent accessible surface area, and binding energy. As a result, the designed compounds (ligands M1 and M2) have shown noteworthy potential as a drug candidate for experimental *in vivo* and *in vitro* testing due to their potential inhibition of breast cancer. Finally, the study of retrosynthesis in this work facilitates the synthesis of drug candidates.

Keywords: ADMET, cancer, molecular docking, molecular dynamics, 3D-QSAR, styrylquinolines, tubulin

* **Corresponding author: Reda EL-Mernissi**, Molecular Chemistry and Natural Substances Laboratory, Faculty of Science, University Moulay Ismail, Meknes, Morocco, e-mail: re.elmernissi@edu.umi.ac.ma

* **Corresponding author: Mohammed Kara**, Laboratory of Biotechnology, Conservation, and Valorization of Natural Resources (LBCVNR), Department of Biology, Faculty of Science Dhar El Mahraz, Sidi Mohamed Ben Abdellah University, Fez, 30000, Morocco, e-mail: mohammed.kara@usmba.ac.ma

Marwa Alaqrbeh: Basic Science Department, Prince Al Hussein bin Abdullah II Academy for Civil Protection, Al-Balqa Applied University, Al-Salt, 19117, Jordan, e-mail: marwaqarbh@hotmail.com, marwa.aqrbeh@bau.edu.jo

Ayoub Khaldan: Molecular Chemistry and Natural Substances Laboratory, Faculty of Science, University Moulay Ismail, Meknes, Morocco, e-mail: ayobkaldan@gmail.com

Omkulthom Al kamaly: Department of Pharmaceutical Sciences, College of Pharmacy, Princess Nourah bint Abdulrahman University, P.O. Box 84428, Riyadh, 11671, Saudi Arabia, e-mail: omalkmali@pnu.edu.sa

Anwar M. Alnakhli: Department of Pharmaceutical Sciences, College of Pharmacy, Princess Nourah bint Abdulrahman University, P.O. Box 84428, Riyadh, 11671, Saudi Arabia, e-mail: amalnklee@pnu.edu.sa

Tahar Lakhli: Molecular Chemistry and Natural Substances Laboratory, Faculty of Science, University Moulay Ismail, Meknes, Morocco, e-mail: tahar.lakhli@yahoo.fr

Abdelouahid Sbai: Molecular Chemistry and Natural Substances Laboratory, Faculty of Science, University Moulay Ismail, Meknes, Morocco, e-mail: sbai.abdelouahid@hotmail.com

Mohammed Aziz Ajana: Molecular Chemistry and Natural Substances Laboratory, Faculty of Science, University Moulay Ismail, Meknes, Morocco, e-mail: a.ajanamohammed@fs.umi.ac.ma

Mohammed Bouachrine: Molecular Chemistry and Natural Substances Laboratory, Faculty of Science, University Moulay Ismail, Meknes, Morocco, e-mail: bouachrine2022et2023@gmail.com

1 Introduction

Cancer develops when cells become abnormal, expand beyond their normal limits, and then spread across the entire body or specific organs [1,2]. It is caused by abnormal cellular activities that characterize cancer, including division, morphogenesis, movement, and signaling [3,4]. Cancer affects all parts of the human body, with breast cancer being the most common type and the second leading cause of death, especially among women [5]. Chemotherapy is one of the most widely used methods for treating different types of cancer. Recently, inhibitors that stop or slow down the growth of cancer cells have been used as promising options for cancer treatment [6,7]. Microtubules consist of α and β tubulin heterodimers. They are a prime target for cancer therapy due to their crucial role in cellular processes such as division, cell shape maintenance, cellular motility, and intracellular transit [8]. The cellular functions of microtubules are based on the polymerization dynamics process, and destabilizing microtubules by decreasing microtubule polymer mass or promoting microtubule polymerization is critical for cell division, therefore controlling cancer progression [9]. Several agents, such as epothilones, paclitaxel, and docetaxel, stabilize the polymeric state of tubulin by inhibiting the polymerization process. Destabilizers and stabilizers impair the dynamics of microtubules and tubulin and halt cells during mitosis, thus resulting in cell death. Over the past decade, microtubule-targeting agents, especially vinca alkaloids and paclitaxel, have been widely used in treating different cancers.

Recently, 2-aryl-trimethoxyquinoline analogs have been reported as tubulin inhibitors, with significant action against breast cancer cells and ovarian carcinoma [10,11]. Quinoline is an alkaloid compound that undergoes secondary metabolism and is frequently used for medical, pharmacological, and biological purposes [12–14]. Natural sources include Berberidaceae, Fumariaceae, Papaveraceae, and Rutaceae plants [15–19]. Quinoline derivatives were used as antihypertensives, antiviruses [20], anticancer [21,22], antimalarial [23], antibiotics [24], antioxidants, antimicrobials, anti-inflammatory [25,26], anti-HIV [27]. For inhibition of cell-free platelet derived growth factor receptor tyrosine kinase (PDGF-RTK) activity [28], and antibacterials [25]. This work investigated previously synthesized 43 styrylquinoline compounds as tubulin polymerization inhibitors targeting human breast cancer by computational methods [11].

Computational chemistry techniques are increasingly being used in pharmaceutical research to accelerate the drug design and discovery process, which can reduce the time and cost of discovery research. Many studies have been conducted to develop anticancer drugs, and some compounds have shown great potential in fighting this disease.

Our work aims to propose new drugs and design anticancer drugs using computational methods. In order to establish a correlation between the characteristic structure of styrylquinoline compounds and inhibitory activity against breast cancer, we used three-dimensional quantitative structure-activity relationship (3D-QSAR). To identify critical interactions, molecular docking was performed between four newly designed styrylquinoline molecules and tubulin receptors on virtual screen top hits. After screening the proposed compounds, we analyzed them for absorption, distribution, metabolism, excretion, and toxicity (ADMET) risk. Finally, we employed molecular dynamics (MD) simulations of 100 ns to investigate the interaction mechanism and conformational changes of the newly designed compounds (M1 and M2) at the binding site of the tubulin protein. Computational chemistry techniques are increasingly being used in pharmaceutical research to accelerate the drug design and discovery process, which can reduce the time and cost of discovery research. Many studies have been conducted to develop anticancer drugs, and some compounds have shown great potential in fighting this disease. Our work aims to propose new drugs and design anticancer drugs using computational methods.

2 Materials and methods

This study utilized 43 styrylquinoline compounds synthesized by Mirzaei *et al.* [11] to create 3D-QSAR models [29]. They have a median inhibitory concentration $IC_{50}(\mu M)$ ranging from 4.12 to 5.95 and are converted to pIC_{50} using the formula ($pIC_{50} = -\log IC_{50}$). The database of 43 styrylquinoline compounds was divided into two groups at random [30]; the first group contains 35 molecules used to create the 3D-QSAR model, and the second group (test) contains 8 compounds utilized for validation (their numbers are marked with a star [*]). The common structure of molecules is shown in Figure 1, and Table 1 displays their pIC_{50} values.

2.1 Minimization and alignment

The sybyl program was used to draw the structure of the compounds [31], and the geometry of these compounds was

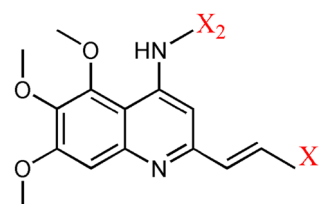
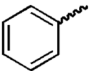
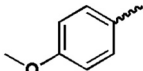
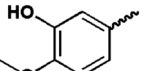
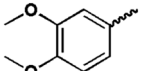
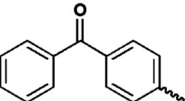
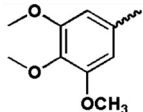
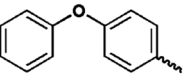
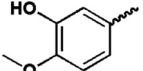
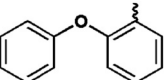
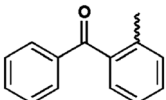
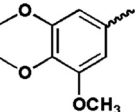
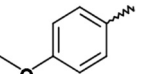
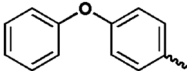
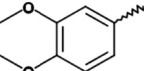
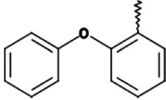
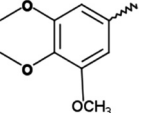
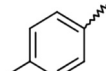
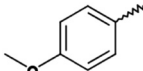
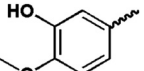
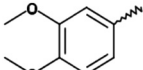
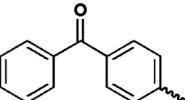
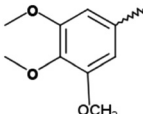
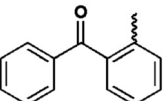
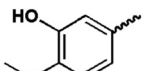
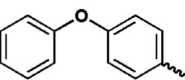
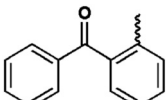
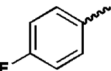
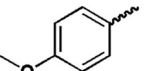
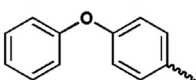
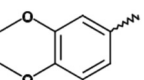
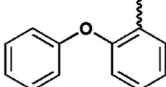
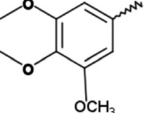
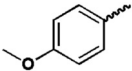
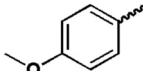
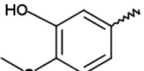
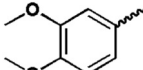
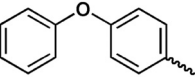


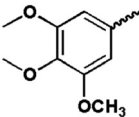
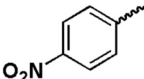
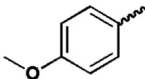
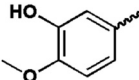
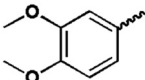
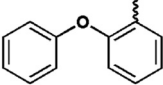
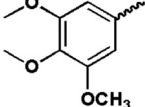
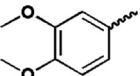
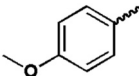
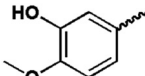
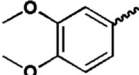
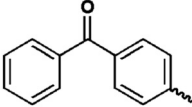
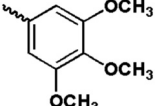
Figure 1: Structure of styrylquinoline derivatives used.

Table 1: pIC_{50} values of studied compounds

N°	X_1	X_2	pIC_{50}	N°	X_1	X_2	pIC_{50}
1*			5.06	23	—		5.59
2	—		5.12	24	—		4.12
3	—		5.30	25	—		5.02
4*	—		5.05	26*	—		5.02
5	—		4.62	27			5.27
6*	—		4.67	28	—		5.35
7	—		4.64	29	—		5.65
8*			5.16	30	—		5.50
9	—		5.27	31	—		4.23
10	—		5.51	32	—		4.31
11*	—		5.19	33	—		4.55
12	—		4.54	34			5.26
13	—		4.85	35*	—		5.42
14	—		4.57	36	—		5.39
15			5.15	37	—		5.29
16	—		5.47	38	—		4.48

(Continued)

Table 1: Continued

N°	X ₁	X ₂	pIC ₅₀	N°	X ₁	X ₂	pIC ₅₀
17	—		5.72	39			
5.08							
18	—		5.36	40	—		5.75
19	—		4.65	41	—		5.61
20			5.62	42	—		5.24
21	—		5.73	43	—		4.96
22	—		5.95				

optimized via a tripos force field with a convergence threshold of 0.01 kcal/mol [32]. Using the alignment technique, the minimized structures were employed as the main conformations to create a trustworthy 3D-QSAR model [33–35]. Compound 22 was used as a template to align all 43 compounds, as shown in Figure 2.

taken into consideration such as the optimum number of components (N), the standard error of estimate (SEE), and F -test value (F). Furthermore, based on a test set, r_{ext}^2 parameter was utilized to determine the best predictive model [41].

2.2 Development of 3D-QSAR models

Comparative molecular similarity indices analysis (CoMSIA) contours were used to construct 3D-QSAR models to explore the relationship between 3D structure and the biological activity of the designed molecules [33,36,37]. CoMSIA contour used steric, electrostatic, hydrogen bond donor (HBD), hydrogen bond acceptor (HBA), and hydrophobic fields to enhance activity [38]. The energy cutoff was set at 30 kcal/mol, and the column filtering value was set at 2.0 kcal/mol, but the rest parameters of the partial least square (PLS) analysis were launched by default. There are parameters to consider while choosing a better model, such as the high values of correlation coefficient R^2 and the coefficient of cross-validation correlation Q^2 ($R^2 > 0.60$ and $Q^2 > 0.50$) [39,40]. Other parameters are

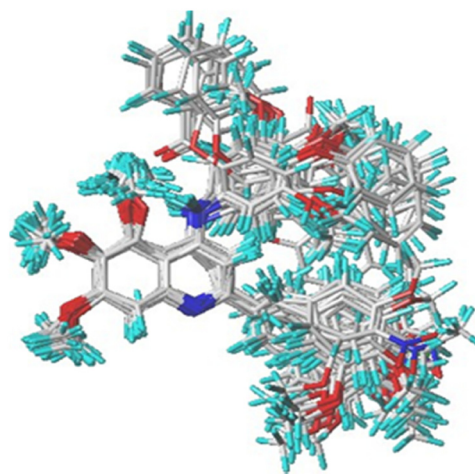


Figure 2: Alignment of molecules.

2.3 Y-randomization test

The Y-randomization method was used to check the correlation between the molecule's structures and their pIC_{50} . The computation of the two parameters q_{Yrand}^2 and r_{Yrand}^2 after each random change in the pIC_{50} is sufficient to assess the model's dependability [38,42].

2.4 Density functional theory (DFT)

The energies of the boundary orbits [43], the lowest unoccupied molecular orbitals (LUMO), and the highest occupied molecular orbitals (HOMO) (E_{LUMO} , and E_{HOMO}) for the proposed compounds were calculated using Gaussian 09 software [44] with DFT and conjugated with the B3LYP/6-31G base [45,46]. E_{HOMO} and E_{LUMO} are used to calculate the following properties; the energy gap $\Delta E_{gap} = (E_{LUMO} - E_{HOMO})$, chemical hardness ($\eta = (\Delta E_{gap})/2$), the chemical potential μ is the first derivative of total energy [47], it is calculated by ($\mu = (E_{LUMO} + E_{HOMO})/2$), electronegativity ($\chi = -\mu$) explains the possibility and character of bond polarization [48], the chemical softness ($S = 1/\eta$), and the global electrophilicity ($\omega = (\mu/2\eta)$) [49].

2.5 Molecular docking

In recent decades, extensive research has been conducted on using tubulins as a biological target in cancer treatment, mainly due to their crucial role in the mitosis process [50]. Various tubulin inhibitors, specifically $\alpha\beta$ -tubulin, have been investigated, revealing four main classes of compounds that bind to specific and corresponding sites: laulimalide, taxane, Vinca alkaloid, and colchicine. For docking with potent molecules, the protein tubulin complex with colchicine (PDB ID: 4O2B) was selected as the ideal target protein [51]. Downloading the protein tubulin (4O2B) from the Protein Data Bank (PDB) is the first step in molecular docking by link (<https://www.rcsb.org>). After that, it is necessary to eliminate water molecules to prepare receptors in their fundamental state. This step is followed by the usage of Surflex-Dock module in Sybyl 2.0, and in the final step, it is necessary to use Discovery and Pymol software [52,53] to determine the types of interactions [54,55].

2.6 ADMET prediction

The pharmacokinetics properties of absorption, distribution, metabolism, excretion, and toxicity are abbreviated in the word ADMET [56,30,38]; the SWISSADME web server has been programmed to determine these properties of the

proposed derivatives (M1–M4) and 22; SWISSADME is a free web application on a website (<http://www.swissadme.ch>), and this step requires in the first step the drawing of these molecules, then the transformation of these structures in the form of codes (SMILES format), pkCSM (<https://biosig.lab.uq.edu.au/pkcsml>) webserver used to provide a set of molecules (SMILES format) [30,38], and in the second step, we put the codes (SMILES format) in the prediction of ADMET properties [54,57,58].

2.7 MD simulations

MD simulations during 100 ns were applied to get an overview of the stability of the [Tubulin–PredM1; Tubulin–PredM2] protein–ligand interaction [59]. The dynamic simulation run was performed based on the best docking position. In order to neutralize the system, Cl^-/Na^+ ions are introduced in this stage. The steepest descent (5,000 steps) was applied to minimize system energy. To check if the system has reached the pressure (1 bar) and temperature (300 K), balancing is applied under an NVT ensemble (constant number of particles N, constant system volume V and constant temperature T) at 298 K. A MD simulation with an NPT ensemble (constant pressure P) was followed to relax and refine the configuration at 1 atm, to stabilize the pressure and temperature of the complexes. Each complex is simulated at a temperature of 300 K for 125 ps, with the use of 40 and 400 $\text{kJ mol}^{-1} \text{nm}^{-2}$ positional restraints on the side chains and the backbone, respectively. In addition, the NPT assembly was used in the production of 100 ns of simulation. The production and equilibration run were obtained during the simulation time by GROMACS 5.0.7 [60], and the complexes [Tubulin–PredM1; Tubulin–PredM2] are subjected to a CHARMM36 force field [61]. The most accentuated descent approach (5,000 cycles) was used for initial minimization by the simulation annealing method. Energy minimization for the entire system is performed at 50,000 energy minimization steps. The Ewald particle mesh method deals with electrostatic interactions with a physiological condition (0.9% NaCl, pH 7.4, 300 K) [62]. After the dynamic simulation duration (100 ns) is complete, the stability of [Tubulin–PredM1; Tubulin–PredM2] complexes was analyzed by root mean square fluctuation and deviation (RMSF and RMSD), number of H bond, solvent accessible surface area (SASA), and radius of gyration (R_g). The g-MMPBSA program was used to estimate the binding free energies (ΔG_{Bind}) of the screened complexes from the molecular mechanics of the Poisson–Boltzmann surface (MM-PBSA).

Generally, the binding free energy can be expressed as

$$\Delta G_{binding} = \Delta G_{complex} - (\Delta G_{protein} + \Delta G_{ligand}),$$

Table 2: The results obtained

Model	R^2	Q^2	F	S_{CV}	r_{ext}^2	N	Fraction				
							Ster	Acc	Elec	Hyd	Don
CoMSIA	0.97	0.84	224.65	0.09	0.91	5	0.06	0.54	0.09	0.20	0.11

where $\Delta G_{\text{complex}}$ represents the total free energy of the complex, $\Delta G_{\text{protein}}$ represents the total free energies of the isolated protein, and ΔG_{ligand} represents the total free energy of ligands in a solvent. To decompose the binding energy, at first ΔE_{MM} , ΔG_{polar} , and $\Delta G_{\text{non-polar}}$ were separately calculated for each residue.

2.8 Retrosynthesis

Retrosynthesis is an essential technique for the organic synthesis of drugs. It facilitates the synthesis of candidate drug molecules by reducing the cost and time of the synthesis process [63]. The current work (spaya.ai) database was used to facilitate the synthesis of compounds M1 and M2 as drug candidates against breast cancer.

2.9 Applicability domain

The Domain of Applicability determines the range in which a compound can be confidently predicted. This analysis aspect is explicitly requested [64]. It should be noted that the QSAR-built model is not intended to be used outside of this domain [65]. There are multiple ways to determine the scope of the quantitative structure-property relationship model, including the “leverage” method. The standardized residuals of the dependent variable vary depending on the leverages, which is the basis of this method. Suppose a compound has leverage that exceeds the threshold $h^* = 3(k + 1)/N$ (where N is the number of molecules in the learning set, and k is the number of descriptors). In that case, that compound is considered adequate for the developed model.

3 Results and discussion

3.1 3D-QSAR analysis

The accuracy of the 3D-QSAR model underwent both internal and external validation. CoMSIA produced the most favorable results with an R^2 value of 0.97, an optimized component of 5,

a Q^2 value of 0.84, an SEE value of 0.09, and an F -test value of 224.65. Additionally, the SEE value was low at 0.09, demonstrating the created model's strong internal predictability. Hydrophobic, electrostatic, steric, HBD, and HBA contributions were 20, 9, 6, 11, and 54%, respectively. The external validation (r_{ext}^2) of CoMSIA reached 0.91. The HBA field has a remarkable role in the CoMSIA model, followed by the hydrophobic field. The statistical results of 3D-QSAR PLS analysis are summarized in Table 2, and the experimental and predicted pIC_{50} of molecules are listed in Table 3. The values of experiments and predictions are closer. Figure 3 shows a regular distribution of styrylquinoline derivatives that target human breast cancer activity values as tubulin polymerization inhibitors.

4 Contour map analysis

The most active compound 22 is used as a reference for building CoMSIA contours.

Table 3: Experimental and predicted values

N°	pIC ₅₀	CoMSIA predicted	N°	pIC ₅₀	CoMSIA predicted
1*	5.06	5.01	23	5.59	5.75
2	5.12	5.07	24	4.12	4.4
3	5.30	5.25	25	5.02	5.22
4*	5.05	5.15	26*	5.02	5.15
5	4.62	4.86	27	5.27	5.12
6*	4.67	4.79	28	5.35	5.45
7	4.64	4.74	29	5.65	5.62
8*	5.16	5.20	30	5.50	5.63
9	5.27	5.18	31	4.23	4.50
10	5.51	5.47	32	4.31	4.49
11*	5.19	5.08	33	4.55	4.85
12	4.54	4.81	34	5.26	5.27
13	4.85	4.91	35*	5.42	5.37
14	4.57	4.70	36	5.39	5.43
15	5.15	5.20	37	5.29	5.42
16	5.47	5.40	38	4.48	4.71
17*	5.72	5.60	39	5.08	5.33
18	5.36	5.48	40	5.75	5.62
19	4.65	4.76	41	5.61	5.75
20	5.62	5.72	42	5.24	5.13
21	5.73	5.65	43	4.96	5.01
22	5.95	5.85			

*: Test molecule.

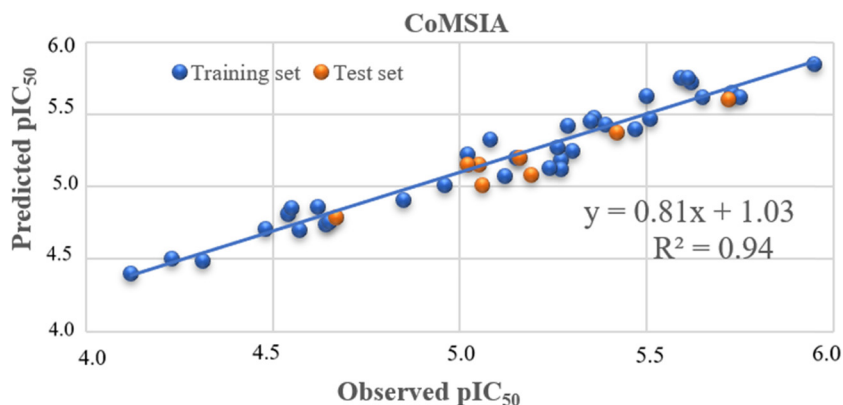


Figure 3: Graphical representation of the observed and predicted activity of training and test sets for CoMSIA models.

4.1 CoMSIA contour maps

The green area of the steric field shown in Figure 4a shows a steric contribution to potency, while the yellow zone decreases potency. A green contour region is visible near two (O–CH₃) groups of *R*₂ substituent, suggesting a preference for small bulky groups that explains the greater biological activity of compound 17 (pIC₅₀ = 5.72) than compounds 16 (pIC₅₀ = 5.47) and 15 (pIC₅₀ = 5.15). Figure 4b shows an electrostatic contour map; the blue contour represents the electronegative charge disfavoring, and the red contour represents the electropositive group disfavoring, respectively. The presence of blue near two (O–CH₃) of *R*₂ and red near the other group (O–CH₃) explains why compound 29 (pIC₅₀ = 5.65) is more active than compound 28 (pIC₅₀ = 5.35) and compound 27 (pIC₅₀ = 5.27). Based on electrostatic and steric fields percents (9 and 6%, respectively), HBD, the hydrophobic fields, and HBA in CoMSIA were examined, as shown in Figure 5a, b, and c, respectively.

HBD (Figure 5a) has a lower stake (11%) than HBA and hydrophobic fields, making them suitable for design in other fields. The cyan and purple in the HBD field indicate favorable and unfavorable conditions for increased activity, respectively. Where H-bond donor groups cause increased activity, as shown by a cyan area around the three –O–CH₃ groups of substituent *R*₂, which explains the higher activity of compound 11 (pIC₅₀ = 5.19) compared to compound 8 (pIC₅₀ = 5.16), and the higher activity of compound 18 (pIC₅₀ = 5.36) compared to compound 13 (pIC₅₀ = 4.85). Figure 5b demonstrates the hydrophobic field; the white and yellow colors represent the hydrophobic parties decrease and increase activity. The *R*₁ and *R*₂ substituents are covered in yellow, meaning water repellency is preferred for increasing activity at these locations. For example, the higher activity of compound 34 (pIC₅₀ = 5.26) compared to compound 8 (pIC₅₀ = 5.16). While the magenta and red colors are shown in Figure 5c of the HBA contour map, they represent HBA groups that can increase and decrease biological activity, respectively. Two substituents,

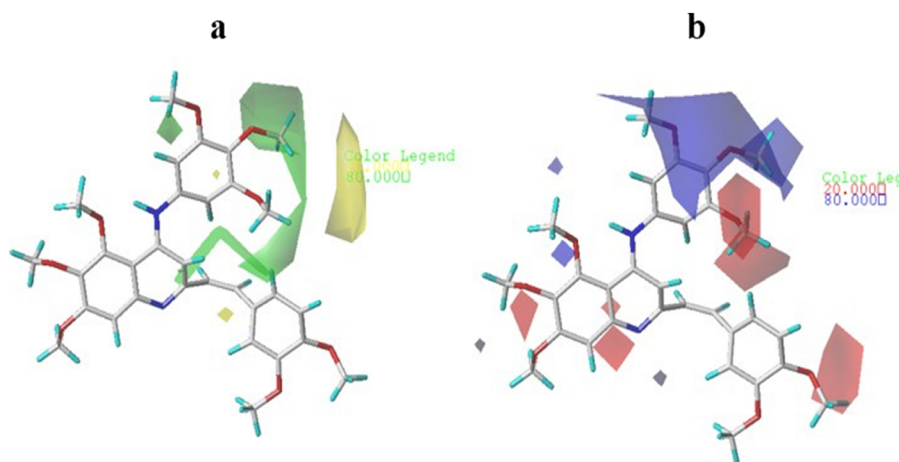


Figure 4: Contour maps of CoMSIA analysis: (a) steric field, and (b) electrostatic field.

Table 4: Result of the Y-randomization test

Iteration	CoMSIA		Iteration	CoMSIA	
	q^2_{Yrand}	r^2_{Yrand}		q^2_{Yrand}	r^2_{Yrand}
1	0.234	0.367	4	0.345	0.356
2	0.453	0.543	5	−0.052	0.121
3	−0.234	0.053	6	0.123	0.321

R_1 and R_2 , with (O–CH₃) covered by magenta, show that this type of HBA group is preferred for increasing activity at these locations, which also explains the higher bioactivity of compound 40 ($pIC_{50} = 5.75$) compared to the bioactivity of compound 21 ($pIC_{50} = 5.73$).

4.2 Y-randomization test

It provides a further understanding of the relationship between the pIC_{50} and the structures of the molecules. The value of pIC_{50} changed randomly to determine the q^2_{Yrand} and r^2_{Yrand} values after each Y-randomization test; the results are listed in Table 4, where the lower values indicate that the correlation is not random.

4.3 Design and prediction

To design new compounds with greater activity than the most active molecule [22], the 3D-QSAR model uses the most important fields to investigate suitable substituents

of styrylquinoline derivatives as tubulin polymerization inhibitors against breast cancer cells. The most contributed fields (HBA) of four newly designed styrylquinoline compounds (M1–M4) have the most tubulin polymerization inhibitory activity, and the pIC_{50} value of compound 22 is lower than the pIC_{50} of the newly designed compounds. Table 5 shows the structures and calculated pIC_{50} of the newly designed compounds.

4.4 DFT

Molecular frontier orbitals can donate and accept electrons. HOMO and LUMO represent the capacity of a compound to donate and withdraw electrons from proposed molecules (M1–M4) electrons, respectively. The unit of energy was measured in the atomic units (au) and then converted to eV (1 au = 27.2113 eV). Table 6 presents the properties computed for proposed compounds in this article, such as hardness η , electronegativity χ , chemical potential μ , energy gap ΔE_{gap} , and electrophilicity ω . The energy gap (ΔE_{gap}) is an important property of designed compounds, giving essential information about these compounds [33]. The smaller the gap energy, the more easily the compound can be excited. The results outlined in Table 6 demonstrate that M1 and M2 have energy gaps of 3.1382 and 3.0604 eV, respectively, indicating that these compounds are less stimulated. This information can be valuable when considering the properties of these compounds for potential applications. The electronegativity and hardness of the proposed compound M1 were found to be 3.9577 and 1.5610 eV, respectively. The LUMO and HOMO energies of the less excited molecule M1 were calculated as

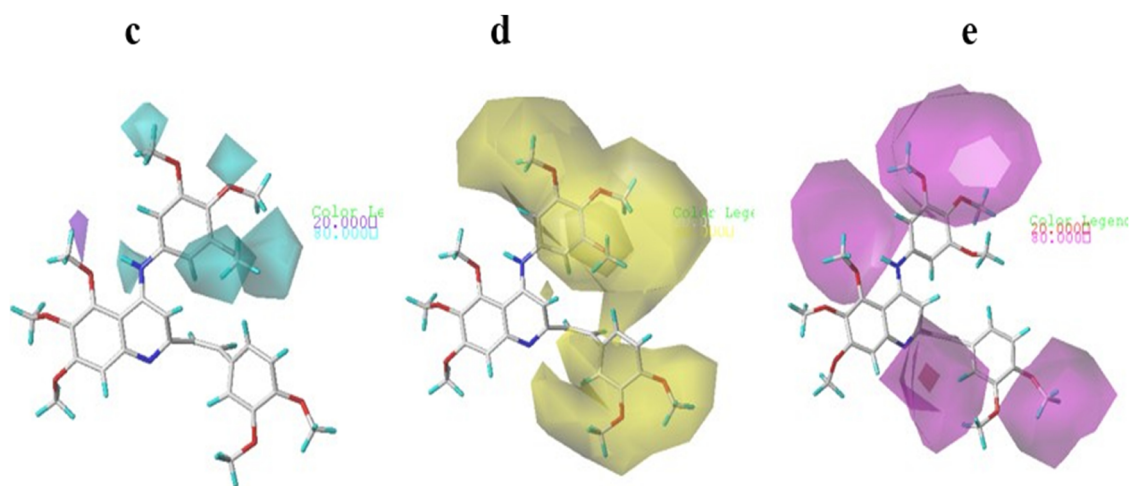
**Figure 5:** Contour maps of CoMSIA: (a) HBD field, (b) hydrophobic field, and (c) HBA field.

Table 5: Newly designed molecules and their predicted pIC_{50}

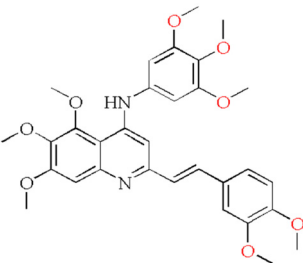
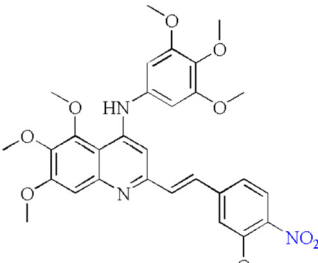
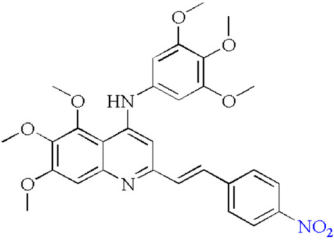
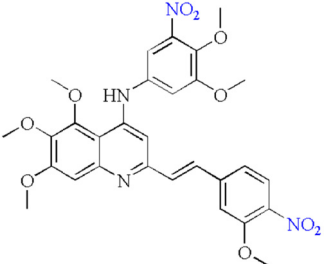
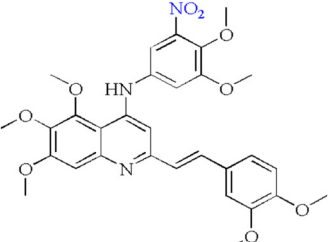
N°	Compounds	Predicted pIC_{50}	N°	Compounds	Predicted pIC_{50}
22		5.80	M3		6.42
M1		6.76	M4		6.14
M2		6.65			

Table 6: Electronic descriptors for the proposed compounds

N°	Global properties (eV)						
	E_{LUMO}	E_{HOMO}	μ	η	χ	ω	ΔE_{gap}
M1	-2.3886	-5.5268	-3.9577	1.5610	3.9577	4.7436	3.1382
M2	-2.1840	-5.2444	-3.7142	1.5302	3.7142	4.5076	3.0604
M3	-2.4756	-5.2085	-3.8420	1.3664	3.8420	5.4014	2.7329
M4	-2.4337	-5.2403	-3.8370	1.4033	3.8370	5.2456	2.8066
22	-2.1739	-5.5301	-3.8520	1.6781	3.8520	4.4210	3.3562

-2.3886 and -5.5268 eV. In contrast, the LUMO and HOMO energies of the designed molecule M2 were calculated as -2.1840 and -5.2444 eV, respectively.

4.5 Molecular docking

$\alpha\beta$ -Tubulin dimers have four distinct interaction sites, including the colchicine-binding site (CBS). This makes CBS a promising target for developing new tubulin modulators.

The tubulin co-crystal ligand was redocked into the binding pocket before the docking investigation to ensure that the docking approach was reliable, as shown in Figure 6. The redocked conformation of 402B was extremely consistent with co-crystallized ligand conformation with an RMSD of 1.388Å (<2.0Å). That indicates that the docking method was reliable and might be used in future research. Molecular docking was used to examine how the newly designed compounds (M1, M2, M3, and M4) and compound 22 bind to the target tubulin–colchicine complex (PDB ID: 402B). The results of the 2D view are listed in Table 7, and the interaction type and total score are listed in Table 8.

The results show that all compounds have favorable interactions, with a total score between 3.45 and 6.53. Compound M1 is the most stable because it has the highest total score of 6.53. The interaction types of M1 with the tubulin protein active site consist of two conventional hydrogen bonds: Asn167 and Ala354, six bonds mixed between carbon H-bonds and Pi-DHB: (Asn258), Tyr202, Ala317, Thr353, Lys352, five Pi sigma/amide-Pi stacked: Leu242, Val238, Leu255, Lys254, and six Pi-alkyl types: Leu252, Ala250, Leu255(4.94), Ala354. Compound M2 has a

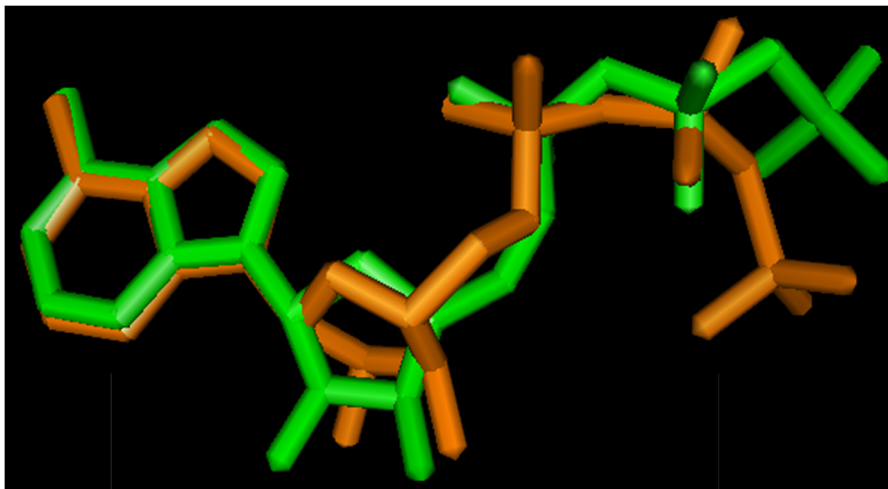


Figure 6: Re-docking pose with the RMSD value of 1.388 Å (green = original, orange = docked).

total score of 5.74 with six different interaction types with the tubulin protein active site consisting of carbon H-bond and Pi-DHB: Val238, Gly237, Asn258, Lys352, one of amide-Pi stacked Lys254, one of Pi-cation Lys254, and five of Pi-alkyl Leu255, Cys241, Ile318, Ala250, Lys352. Moreover, compound M3 has a total score of 4.43 and has four carbon-hydrogen bonds: Gln247, Asn249, Asn350, Val238, one of amide-Pi stacked Leu248; one of Pi-cation type Met259; and three of Pi-Alkyl Ala316, Gys241, Leu248. The binding mode of compound M4 revealed that it bonds inside the binding pocket with a total score of 3.67 and has four types of carbon-hydrogen bond interaction Thr353, Gln247, Asp251, one Pi-Sigma (Leu255), one Pi-cation (Lys254), and three types of pi-alkyl interaction Ala250, Lys352, and Leu 248. Compound 22 has a total energy of 3.45 with three types of carbon-hydrogen bond interactions: Asn349, Asn350, one interaction of type Pi-sigma Leu255, one interaction of type Pi-cation Lys254, and three interactions of type Pi-Alkyl Ala250, Lys352.

These compounds are more stable than the reference compound 22, which has a total score of 3.45. It has two interactions of type carbon-hydrogen bond interaction (Asn349, Asn350), one interaction of type Pi-sigma (Asn258), and two mixed interactions between Pi-alkyl and alkyl (Leu248, Cys241). Additionally, molecular docking studies indicated that compounds M1 and M2 have a strong affinity for the CBS of tubulin and could serve as lead molecules for future pharmaceuticals.

4.6 ADMET prediction

Computational pharmacology (ADMET) is a rapidly growing field that includes developing software to integrate and capture medical and biological data worldwide. It is important

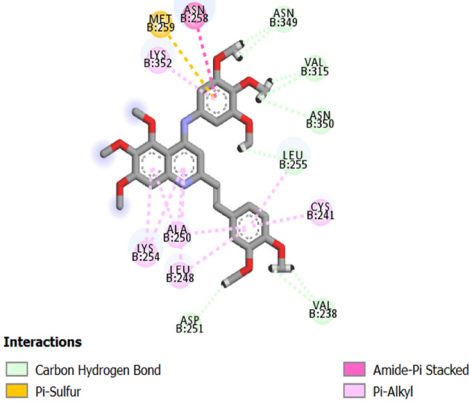
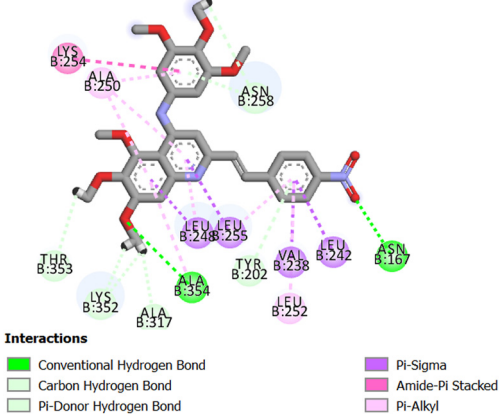
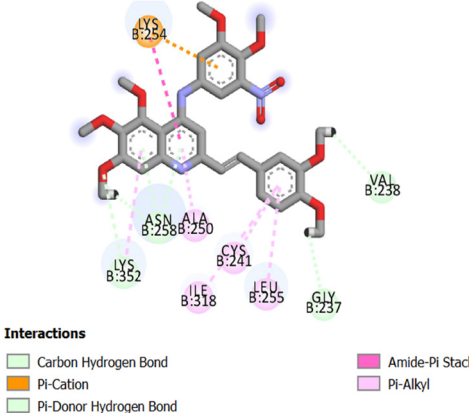
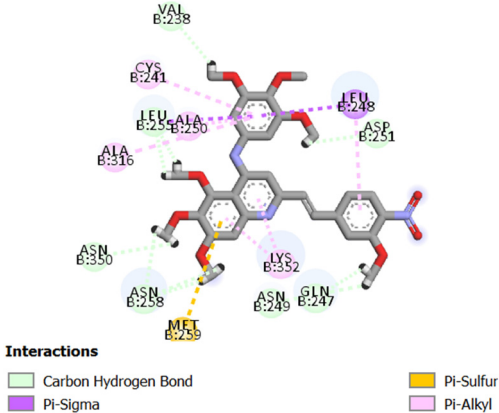
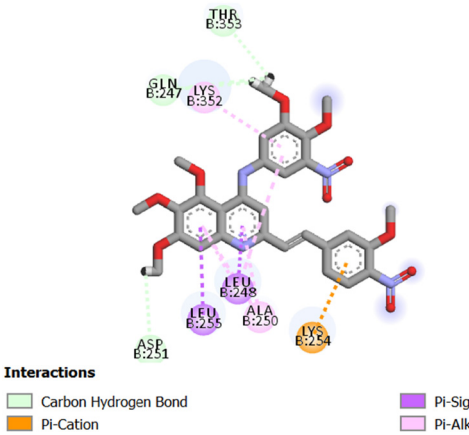
to study the ADMET properties of compounds, which can be done using *in silico* techniques, to find and create new medicines. Table 9 shows the ADMET prediction. The results show that all the compounds have an absorbance value of almost 90%, which means the human intestine absorbs them well. The blood-brain barrier (BBB) protects the brain and maintains good health. Furthermore, it blocks the flow of hazardous chemicals, preventing them from easily entering the brain; all designed compounds have a log BB value < -1 [66,67], and they cross the BBB poorly. The second parameter is the volume of distribution (VDss), which measures the intensity of drug diffusion in the body; the values are not accepted if (VDss) < -0.15 and are considered low, while compounds with VDss > 0.45 are accepted and have a high distribution. All designed compounds (M1, M2, M3, and M4) have VDss > 0.45 .

Drug detoxification and elimination is an essential stage in metabolism; many cytochromes are involved, including 2D6, 3A4, 1A2, 2C19, 2C9, 2D6, and 3A4. All newly designed compounds (M1, M2, M3, and M4) were shown to be CYP3A4 inhibitors and substrates, but they are inhibitors only of 1A2 and 2C19 in this research. Constant clearance describes the relationship between drug concentration in the body and drug removal rate; when the clearance value is higher, the medication is considered safe. All designed compounds have a higher clearance value and are not toxic, making them the best-designed drug treatment against human breast cancer cells.

4.7 MD simulation

Under normal pressure and temperature conditions, the MD simulations were run for 100 ns for the best-newly

Table 7: 2D view of the binding conformation for the newly designed compounds (M1, M2, M3, and M4) and compound 22 with the target tubulin–colchicine complex (PDB ID: 4O2B)

N°	2D view	N°	2D view
22		M1	
STRM2		M3	
M4			

designed compounds M1 and M2 with tubulin protein active site (PredM1 and PredM2) complexes on the “C-alpha position.” They demonstrated the best stability at molecular docking, and the results during dynamic simulation showed that the ligands (PredM1 and PredM2) remain bound to the protein (tubulin (pocket. Calculations of

RMSD, RMSF, R_g , hydrogen bonding, SASA, and average center of the mass distance between protein–ligand and binding free energy (MMPBSA) were carried out to assess the stability of each structure.

All the proposed complexes [Tubulin–PredM1; Tubulin–PredM2] showed good stability in 100 ns simulation.

Table 8: Interaction types and total score of the newly designed compounds (M1, M2, M3, and M4) and compound 22 with the target tubulin–colchicine complex

N°	Types of interactions			Total score
	Carbon H-bond, Pi-DHB, conventional hydrogen bond	Pi-sigma, amide-Pi stacked, Pi-sulfur, Pi-cation	Pi-alkyl, alkyl	
22	Asn349, Asn350	Asn258	Leu248, Cys241	3.45
M1	Asn167, Asn258, Tyr202, Ala317, Lys352, Thr353, Ala354	Leu242, Val238, Leu255, Lys254	Leu252, Ala250, Leu255, Ala354	6.53
M2	Gly237, Val238, Lys352, Asn258	Lys254	Leu255, Cys241, Ile318, Ala250, Lys352	5.74
M3	Gln247, Asn249, Asn350, Val238	Leu248, Met259	Ala316, Gys241, Leu248	4.43
M4	Thr353, Gln247, Asp251	Leu255, Lys254	Ala250, Lys352	3.67

Table 9: ADMET prediction of the most potent (C22) and the newly designed

Model	Compounds				
	22	M1	M2	M3	M4
(A)					
Intestinal absorption (human)	83.90	89.95	98.42	86.70	87.23
(D)					
VDss (human)	0.35	0.46	0.49	0.56	0.52
BBB (logBB)	−0.984	−1.08	−1.41	−1.28	−1.45
(M)					
Inhibition (CYP)	2C19	+	+	+	+
	2D6	−	−	−	−
	3A4	+	+	+	+
	2C9	+	+	+	+
	1A2	−	−	−	−
Substrate (CYP)	3A4	+	+	+	+
	2D6	−	−	−	−
(E)					
Clearance	0.62	0.40	0.45	0.65	0.66
(T)					
AMES toxicity	−	−	−	−	−

Abbreviation symbol: A: Absorption, D: Distribution, VDss: Volume of distribution, BBB: Blood–brain barrier, M: Metabolism, E: Excretion, T: Toxicity, +: Yes, −: Non.

4.8 RMSD

All complex configurations' stability was studied using the RMSD during 100 ns MD simulation. Figure 7 shows RMSD for (PredM1 and PredM2); the RMSD of PredM1 ligand reaches its maximum value but is less than 40 ns during the first 30 s; after 40 ns, the graphs of M1 ligands and the protein need clarification during simulation. In the pred M2, generally, the whole chart remains stable during simulations (100 ns), and the RMSD values for the complex reach 2 Å. Generally, backbone RMSD stabilizes after 40

ns for the (Tubulin–PredM1) complex and after 10 ns for the (Tubulin–PredM2) complex. The average values of the backbone RMSD for M1 and M2 are 1.9 ± 0.3 and 1.3 ± 0.17 Å, respectively. Generally, all deviations of proteins, ligands, and complexes are less than 4 Å; this indicates the proteins, ligands, and complexes are stable in the majority time of simulation dynamics.

4.9 RMSF

RMSF was utilized to evaluate the average fluctuation of the overall structure for each amino acid in the protein or to identify a flexible protein region. Figure 8 shows the RMSF graphs for the two complexes (Tubulin–PredM1, Tubulin–PredM2). In the graph of Pred M2, five peaks appear at the residue numbers 50, 180, 280, 380, and 440, while in the complex Pred M1, a peak appears at the 380 residues. As a result, the (Tubulin–PredM1) complex is more adaptable and of higher quality than the (Tubulin–PredM2) complex. The fluctuation intensity remains below 3.0 Å for both complexes except for some residues representing loops or turns in the protein (Tubulin). The (Tubulin–PredM2) complex has lower RMSF values than (Tubulin–PredM1), which indicates a better effect the ligand has on stabilizing protein (Tubulin) residues than M1. Generally, the RMSF of all complexes (Tubulin–PredM1, Tubulin–PredM2) are significantly similar, and all graphs of RMSF characteristics show less fluctuation, which indicates excellent stability of the two complexes. In addition, the appearance of the same amino acids in molecular docking and dynamic simulations as Asn167, Tyr202, Leu242, Asn258, Ala317, Lys352, Thr353, and Ala354 complex (Tubulin–PredM1) and Gly237, Val238, Leu255, Asn258, and Ile318 for (Tubulin–PredM2). The molecular simulation dynamics results indicate that all docking molecular results are validated.

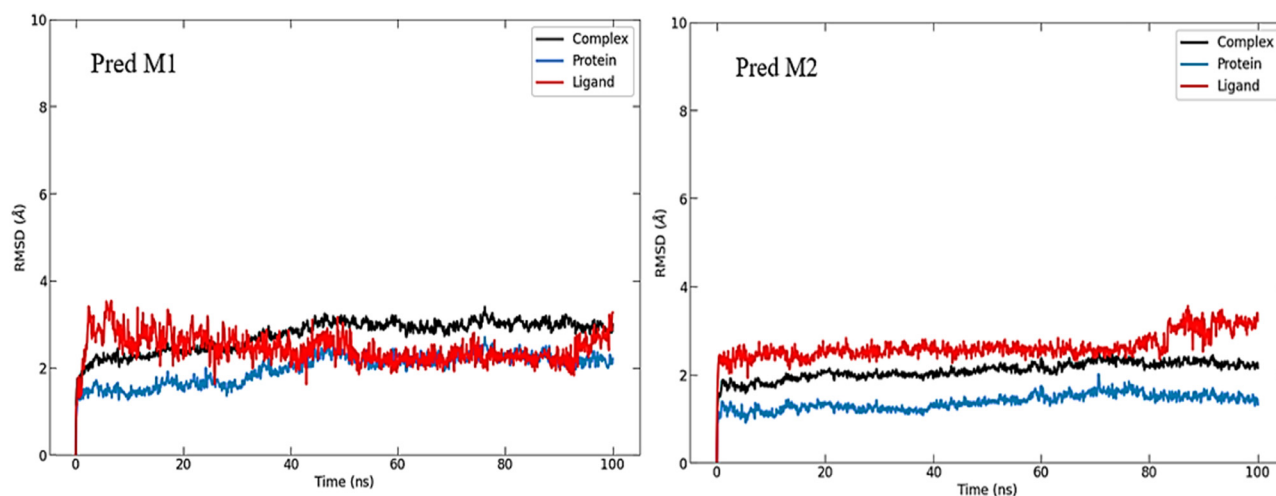


Figure 7: RMSD graphs of the complex, protein (Tubulin), and ligands (M1, M2) according to the simulation.

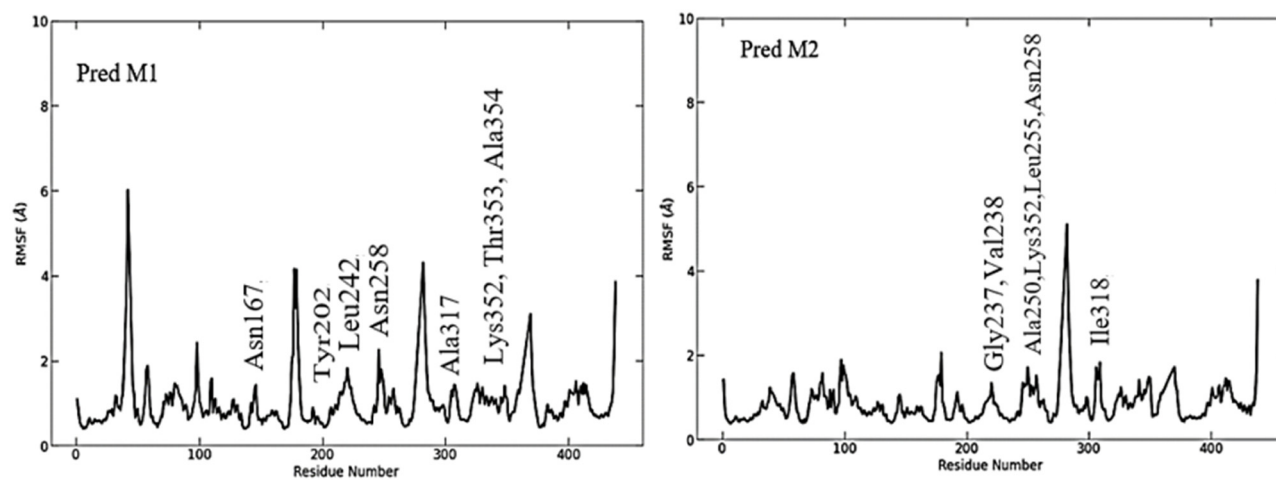


Figure 8: Flexibilities of the protein backbones examined by RMSF values.

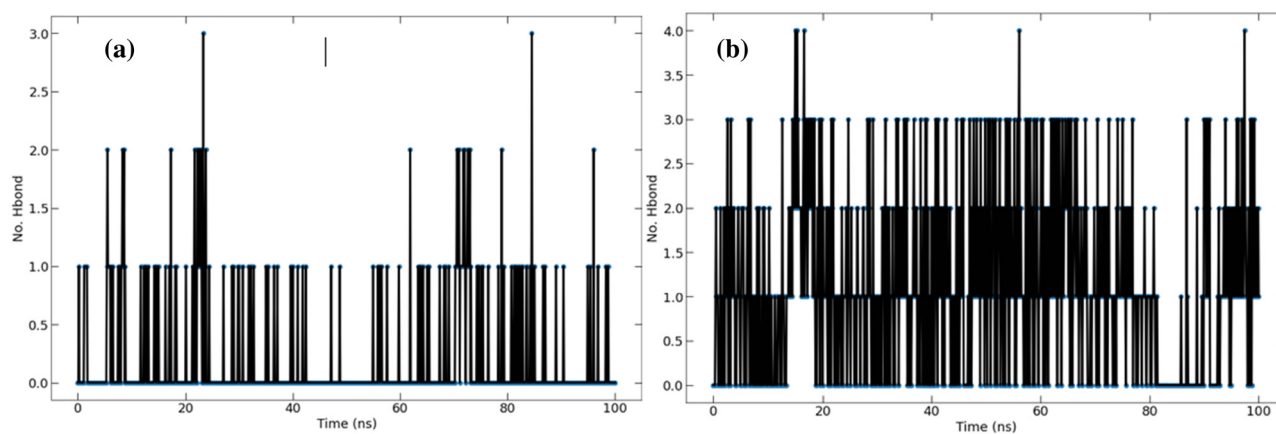


Figure 9: (a) and (b) Hydrogen bonds of complex (Tubulin–PredM1) and (Tubulin–PredM2), respectively.

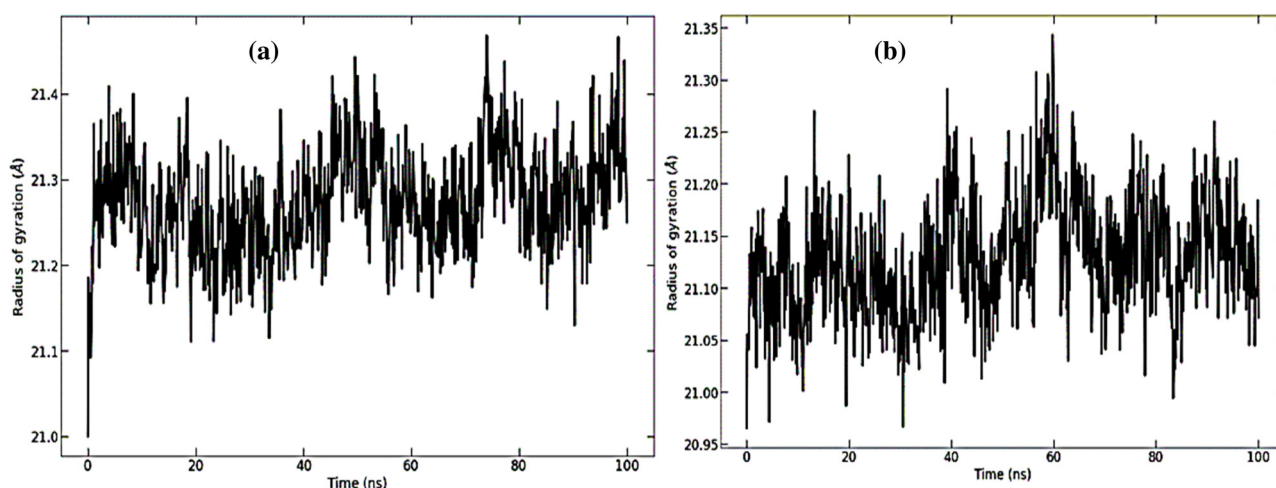


Figure 10: (Tubulin–PredM1) (a) and (Tubulin–PredM1) (b) R_g of the complexes during 100 ns MD simulation.

4.10 Hydrogen bond

The total number of hydrogen bonds and average center-of-mass distance formed between the ligand (M1, M2) and protein (Tubulin) are shown in Figure 9. For the (Tubulin–PredM1) complex, the maximum number of hydrogen bonds reaches three at 25 and 85 ns, respectively. After that, this number reaches two hydrogen bonds at 6, 8, 18, 22–24, 62, 71–73, 78, and 98 ns. In the rest of the simulation, this number reaches 1. Generally, ligand M1 has H-bond gaps throughout most of the simulation time, even though the ligand is stable in the binding site. For the (Tubulin–PredM2) complex, the maximum number of hydrogen bonds reaches four at 16, 18, 58, and 98 ns. After that, this number reaches three, two, and one hydrogen bonds for the rest of the simulation. Ligand M2 forms a stable hydrogen bond network with the protein (Tubulin) over the simulation time.

4.11 R_g

R_g is linked to the conformational state to show if a structure is folded and compact and has a stable conformation. The smaller the R_g value, the less flexible the proteins and the more stable the complexes. According to Figure 10, low R_g values for PredM1 (A) and PredM2 (B) led us to believe they were stable. R_g in the simulation was used to determine the compactness of the structure. The consistency throughout the simulation and the lower degree of fluctuation during the simulation indicate that the system is more rigid and compact. Both complexes (Tubulin–PredM1) and (Tubulin–PredM2) have the lowest R_g values, 21.13 and 20.97 Å, respectively. The R_g values varied between 21.13 and 21.43 Å for (Tubulin–PredM1) complexes and between 20.97 and 21.35 Å for (Tubulin–PredM2) complexes. In conclusion, all complexes showed relatively similar consistent R_g and compactness values, indicating they have good stability.

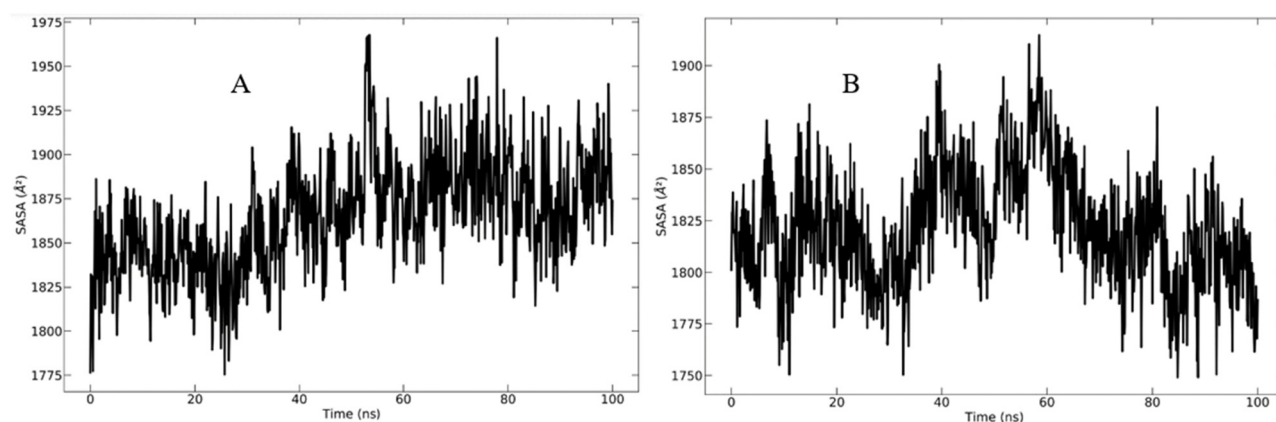


Figure 11: SASA for 100 ns of the simulations. (a) and (b) represent Tubulin–PredM1 and Tubulin–PredM2, respectively.

Table 10: Binding free energies of predicted compounds (kJ/mol)

Energy (kJ/mol)		Ligands	
		M1	M2
ΔE_{MM}	Van der Waal	-151.658 ± 38.652	-187.563 ± 32.693
	Electrostatic	-29.702 ± 41.002	-51.128 ± 30.186
ΔG_{Sol}	Polar solvation	98.050 ± 33.839	152.559 ± 68.591
	ΔG_{SASA}	-18.464 ± 3.421	-22.222 ± 3.487
Binding (ΔG_{bind})		-101.775 ± 26.749	-108.355 ± 77.540

4.12 SASA

The magnitude of conformational changes that the water solvent can access was predicted using the graphs of SASA of the complexes (Tubulin–PredM1; Tubulin–PredM2). Hence, the interaction between these complexes and the solvent during the 100 ns MD simulation was analyzed using the SASA, as shown in Figure 11a. Figure 11a shows an SASA value varying between 1,825 and 1,875 Å² for Tubulin–PredM1 in the first 50 ns of simulations. However, after 50 ns, the solvent-accessible surface area varied between 1,850 and 1,925 Å², indicating that the surface reached in the second period and remained stable. On the other hand, Figure 11b revealed values between 1,800 and 1,850 Å² in the first 38 ns. After the simulation interval [38–65 ns], the SASA value increases, reaching 1,825 and 1,875 Å². In the rest

of the simulation [66–100 ns], this value slowly decreases and varies between 1,800 and 1,850 Å². The solvent-accessible zone reached by the [Tubulin–PredM1] complex is substantially similar to the zone reached by the [Tubulin–PredM1] complex; this value is higher and is very important, and SASA values for these two complexes (Tubulin–PredM1; Tubulin–PredM2) remain relatively stable, which indicates no significant changes during a 100 ns simulation.

4.13 Binding energy calculation

MM/PBSA determines how stable newly designed compounds are for binding to tubulin proteins, using the fastest force field to calculate the free energy. The different types of energies calculated by the MM-PBSA method during 100 ns of simulation are listed in Table 10. The average binding free energies of (Tubulin–PredM1) and (Tubulin–PredM2) complexes calculated were found to be -101.775 ± 26.749 and -108.355 ± 77.540 kJ/mol, respectively. The average ΔE_{MM} for (Tubulin–PredM1) and (Tubulin–PredM2) complexes were found to be -181.36 ± 79.654 and -238.691 ± 62.879 kJ mol⁻¹, respectively. The average values of ΔG_{Polar} for the (Tubulin–PredM1) and (Tubulin–PredM2) complexes were -18.464 ± 3.421 kJ/mol and -22.222 ± 3.487 kJ/mol, respectively. The calculated average ΔG_{SASA}

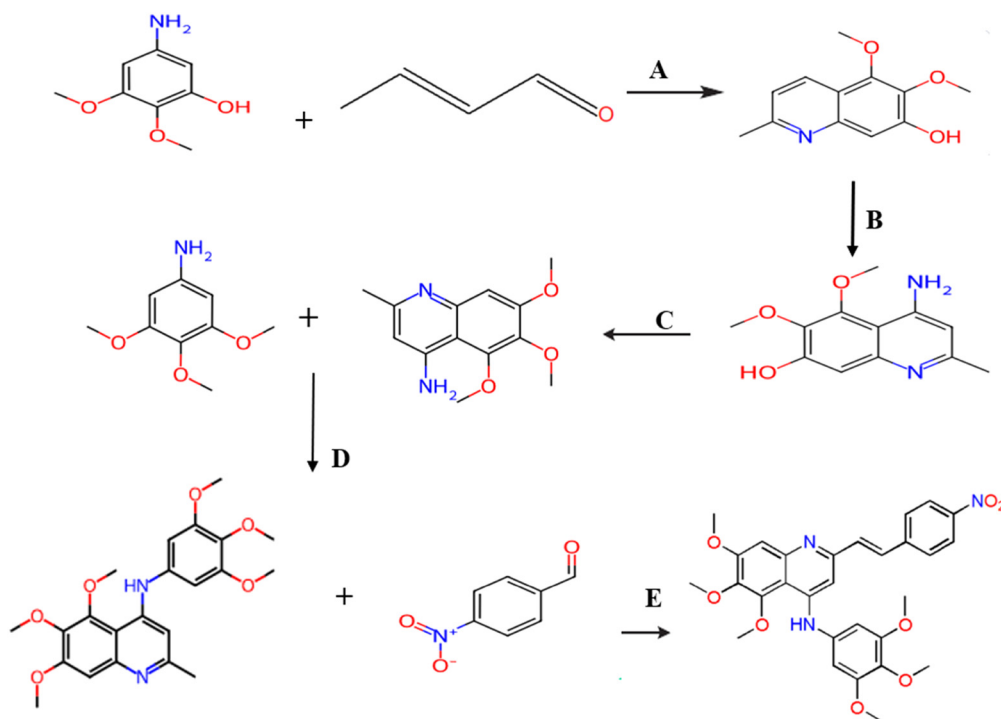
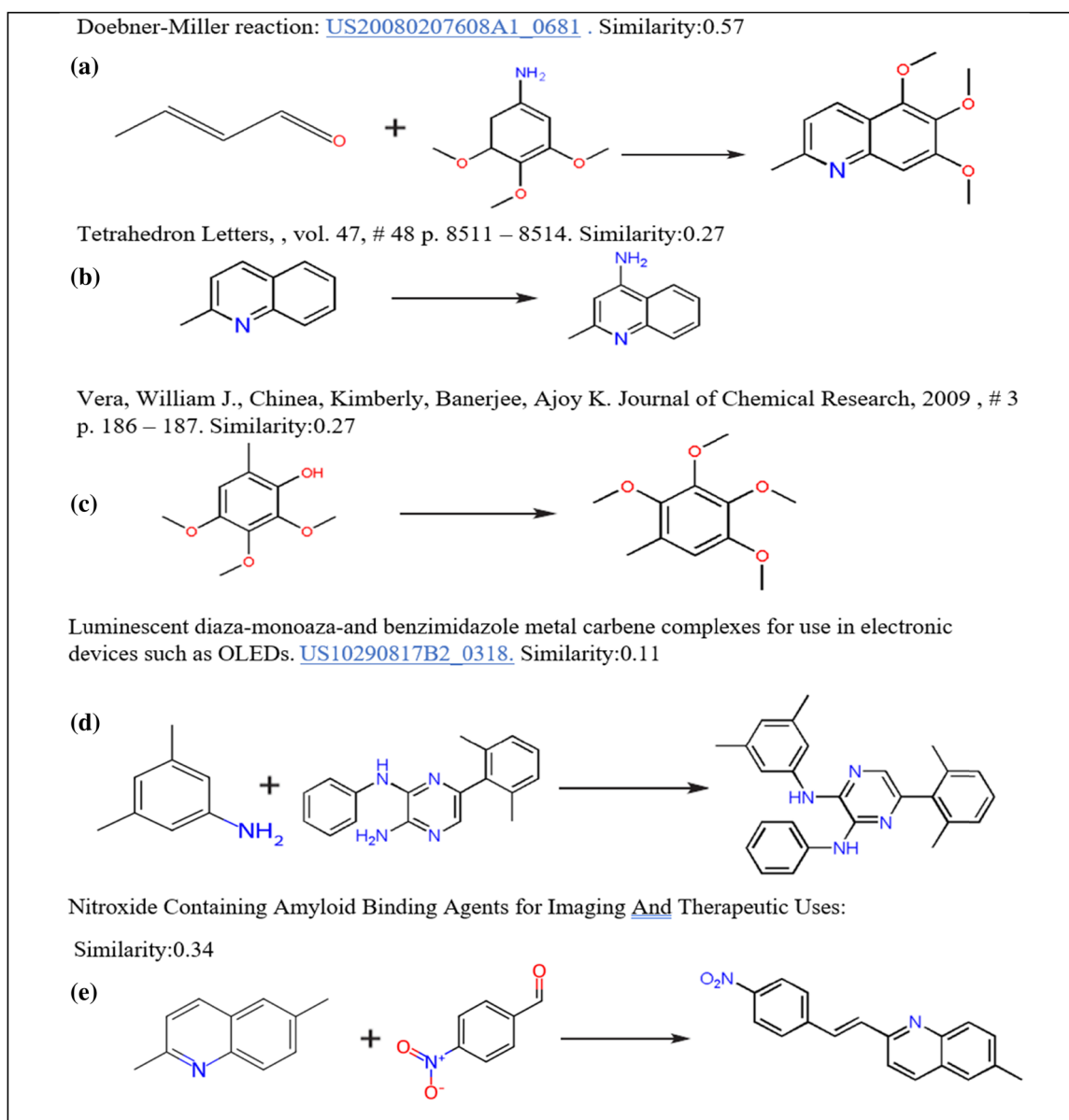
**Scheme 1:** The different stages of the prepared compound M1.

Table 11: Reactions for the synthesis of compound M1

for (Tubulin–PredM1) and (Tubulin–PredM2) complexes were -18.464 ± 3.421 and 22.222 ± 3.487 kJ/mol, respectively. From the MM-PBSA result, we notice that all complexes showed almost closer values; this indicates good and excellent stability of our complexes.

4.14 Retrosynthesis analysis

Based on the retrosynthesis methods, the Spaya platform (<https://www.spaya.ai>) facilitates the synthesis of drug

candidates with a high total score. Each route is a collection of similar synthetic steps documented in the literature (Scheme 1 and Table 11).

4.15 Applicability domain

Figure 12 shows the standardized prediction errors as a function of the lever values (hi) of the molecules in training, test sets, and the proposed M1 and M2 molecules.

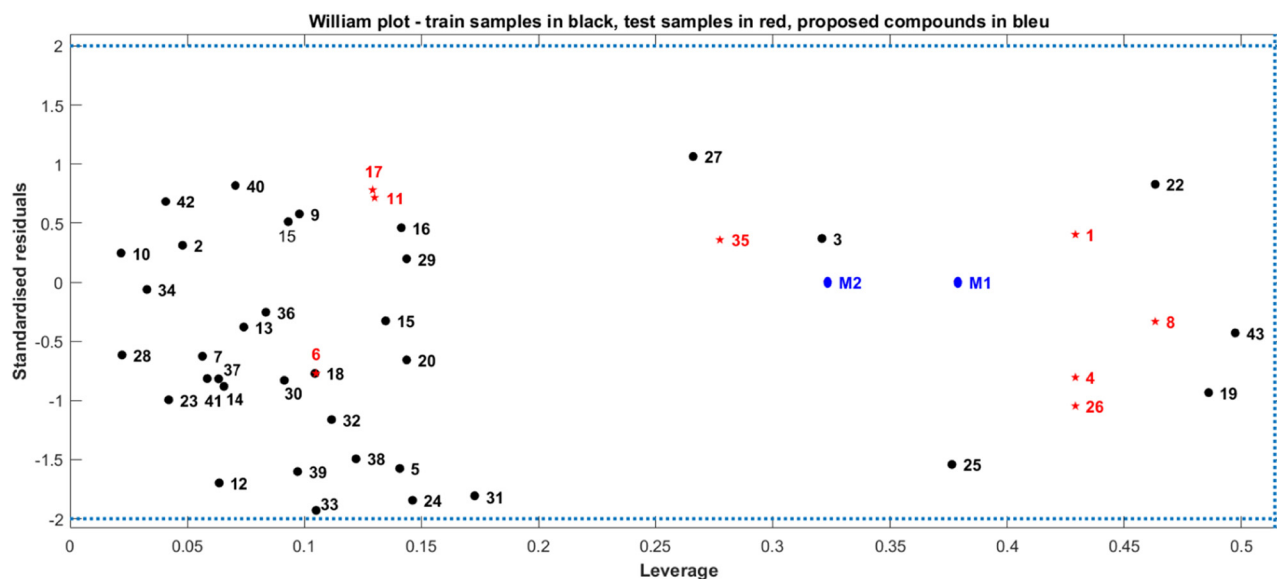


Figure 12: Williams plot to evaluate the applicability domain of the model ($h^* = 0.53$ and residual limits = ± 2).

All compounds have levers $h_i < h^* = 0.53$, and all the tailings including M1 and M2 are found to be in the range of (2SD) (horizontal lines); this explains is a reliable model.

5 Conclusion

This work uses various *in silico* techniques, such as 3D-QSAR/CoMSIA, molecular Docking, ADMET, MD, MM-PBSA binding energy calculations, and retrosynthesis. In order to examine and identify the essential designed compounds for tubulin inhibition against human breast cancer. The statistical results ($Q^2 = 0.84$, $R^2 = 0.97$, $r_{\text{ext}}^2 = 0.91$) obtained from the best CoMSIA-HA model are reasonable, predictive, and reliable, which gives credibility to the molecules designed (M1, M2, M3, and M4). Molecular docking was used to predict the interaction types and total score of all designed compounds at the active site of tubulin protein. The designed styrylquinolines compounds (M1 and M2) showed great stability and demonstrated excellent pharmacokinetic characteristics (ADMET). Moreover, MD simulations combined with free energy evaluated the stability of compounds M1 and M2. Therefore, the two proposed compounds (M1 and M2) were found to be more stable in the tubulin protein binding site.

It is important to synthesize these compounds, which may be useful in developing tubulin polymerization inhibitors against human breast cancer candidate drugs.

Acknowledgements: The authors extend their appreciation for Princess Nourah bint Abdulrahman University Researchers Supporting Project number (PNURSP2024R489) Princess Nourah bint Abdulrahman University, Riyadh, Saudi Arabia.

Funding information: The research was finically supported by Princess Nourah bint Abdulrahman University Researchers Supporting Project number (PNURSP2024R489) Princess Nourah bint Abdulrahman University, Riyadh, Saudi Arabia.

Author contributions: R.E.M., M.A., A.K., M.A.A., and M.B.: methodology; formal analysis; R.E.M., A.K., and M.K.: writing-review and editing; R.E.M., O.A., A.M.A and M.K.: software, project administration, resources, R.E.M., T.L., A.S and M.A.A.: writing-original; M.A.A., and M.B.: supervision, review and editing, R.E.M., M.A.A., A.M.A., and M.B.: conceptualization. All authors have read and agreed to the published version of the manuscript.

Conflict of interest: The authors declare no conflict of interest.

Ethical approval: The conducted research is not related to either human or animal use.

Data availability statement: The datasets generated during and/or analyzed during the current study are available from the corresponding author on reasonable request.

References

- [1] Rashmi S, Kamala S, Murthy S, Kotha S, Rao Y, Chaudhary K. Predicting the molecular subtype of breast cancer based on mammography and ultrasound findings. *Indian J Radiol Imaging*. 2018;28(3):354–61.
- [2] Siegel RL, Miller KD, Jemal A. Cancer statistics, 2019. *CA A Cancer J Clin*. 2019 Jan;69(1):7–34. doi: 10.3322/caac.21551 [cited 2023 Oct 6].
- [3] Sana S, Tokala R, Bajaj DM, Nagesh N, Bokara KK, Kiranmai G, et al. Design and synthesis of substituted dihydropyrimidinone derivatives as cytotoxic and tubulin polymerization inhibitors. *Bioorg Chem*. 2019 Dec;93:103317, <https://linkinghub.elsevier.com/retrieve/pii/S0045206819307928>. [cited 2021 Apr 8].
- [4] Sun M, Xu Q, Xu J, Wu Y, Wang Y, Zuo D, et al. Synthesis and bioevaluation of N,4-diaryl-1,3-thiazole-2-amines as tubulin inhibitors with potent antiproliferative activity. *PLoS One*. 2017;12(3):e0174006.
- [5] Fan L, Goss PE, Strasser-Weippl K. Current status and future projections of breast cancer in Asia. *Breast Care (Basel)*. 2015 Dec;10(6):372–8.
- [6] Ceramella J, Caruso A, Occhiuzzi MA, Iacopetta D, Barbarossa A, Rizzuti B, et al. Benzothienoquinazolinones as new multi-target scaffolds: Dual inhibition of human Topoisomerase I and tubulin polymerization. *Eur J Med Chem*. 2019 Nov;181:111583.
- [7] Sultana F, Shaik S, Nayak V, Hussaini S, Marumudi K, Sridevi B, et al. Design, synthesis and biological evaluation of 2-anilinopyridyl-linked oxindole conjugates as potent tubulin polymerisation inhibitors. *ChemistrySelect*. 2017 Oct;2:9901–10.
- [8] Sakchaisri K, Kim SO, Hwang J, Soung NK, Lee KH, Choi TW, et al. Anticancer activity of a novel small molecule tubulin inhibitor STK899704. *PLoS One*. 2017;12(3):e0173311.
- [9] Wloga D, Joachimiak E, Fabczak H. Tubulin post-translational modifications and microtubule dynamics. *Int J Mol Sci*. 2017 Oct;18(10):2207 <https://www.ncbi.nlm.nih.gov/pmc/articles/PMC5666887/>. [cited 2022 Aug 12].
- [10] Dyrager C, Wickström M, Fridén-Saxin M, Friberg A, Dahlén K, Wallén EAA, et al. Inhibitors and promoters of tubulin polymerization: synthesis and biological evaluation of chalcones and related dienones as potential anticancer agents. *Bioorg Med Chem*. 2011 Apr;19(8):2659–65.
- [11] Mirzaei S, Eisvand F, Hadizadeh F, Mosaffa F, Ghasemi A, Ghodsi R. Design, synthesis and biological evaluation of novel 5,6,7-trimethoxy-N-aryl-2-styrylquinolin-4-amines as potential anticancer agents and tubulin polymerization inhibitors. *Bioorg Chem*. 2020 Feb;98:103711.
- [12] Abadi AH, Hegazy GH, El-Zaher AA. Synthesis of novel 4-substituted-7-trifluoromethylquinoline derivatives with nitric oxide releasing properties and their evaluation as analgesic and anti-inflammatory agents. *Bioorg Med Chem*. 2005 Oct;13(20):5759–65. doi: 10.1016/j.bmc.2005.05.053. [cited 2022 Jun 15].
- [13] Kara M, Assouguem A, Kamaly OMA, Benmessaoud S, Imtara H, Mechache H, et al. The impact of apple variety and the production methods on the antibacterial activity of vinegar samples. *Molecules*. 2021 Jan;26(18):5437, <https://www.mdpi.com/1420-3049/26/18/5437>. [cited 2021 Sep 7].
- [14] El Khomsi M, Kara M, Hmamou A, Assouguem A, Al Kamaly O, Saleh A, et al. In vitro studies on the antimicrobial and antioxidant activities of total polyphenol content of cynara humilis from moulay yacoub area (morocco). *Plants*. 2022 Jan;11(9):1200, <https://www.mdpi.com/2223-7747/11/9/1200>. [cited 2022 Jun 17].
- [15] Srivastava V, Negi AS, Kumar JK, Gupta MM, Khanuja SPS. Plant-based anticancer molecules: A chemical and biological profile of some important leads. *Bioorg Med Chem*. 2005 Nov;13(21):5892–908, <https://linkinghub.elsevier.com/retrieve/pii/S0968089605005171>. [cited 2022 Oct 4].
- [16] Byler KG, Wang C, Setzer WN. Quinoline alkaloids as intercalative topoisomerase inhibitors. *J Mol Model*. 2009 Dec;15(12):1417–26.
- [17] Kara M, Assouguem A, Abdou RZ, Bahhou J. Phytochemical content and antioxidant activity of vinegar prepared from four apple varieties by different methods. *TJNPR*. 2021 Oct;5(9):1578–85, <http://tjnpr.org/viewarticle.aspx?articleid=1845>. [cited 2022 Jan 10].
- [18] Hmamou A, Eloutassi N, Alshawwa SZ, Al Kamaly O, Kara M, Bendaoud A, et al. Total phenolic content and antioxidant and antimicrobial activities of papaver rhoeas L. organ extracts growing in taounate region, Morocco. *Molecules*. 2022 Jan;27(3):854, <https://www.mdpi.com/1420-3049/27/3/854>. [cited 2022 Jun 17].
- [19] Hmamou A, Kara M, Khomsi ME, Saleh A, Al Kamaly O, Bendaoud A, et al. Comparative study on the total phenolics, total flavonoids, and biological activities of papaver rhoeas L. extracts from different geographical regions of Morocco. *Appl Sci*. 2023 Jan;13(4):2695, <https://www.mdpi.com/2076-3417/13/4/2695>. [cited 2023 Feb 23].
- [20] Muruganantham N, Sivakumar R, Anbalagan N, Gunasekaran V, Leonard JT. Synthesis, anticonvulsant and antihypertensive activities of 8-substituted quinoline derivatives. *Biol Pharm Bull*. 2004 Oct;27(10):1683–7.
- [21] Chen M, Chen H, Ma J, Liu X, Zhang S. Synthesis and anticancer activity of novel quinoline–docetaxel analogues. *Bioorg Med Chem Lett*. 2014 Jul;24(13):2867–70, <https://www.sciencedirect.com/science/article/pii/S09680894X1400448X>. [cited 2022 Dec 4].
- [22] Pettit GR, Lippert JW. Antineoplastic agents 429. Syntheses of the combretastatin A-1 and combretastatin B-1 prodrugs. *Anticancer Drug Des*. 2000 Jun;15(3):203–16.
- [23] LaMontagne MP, Markovac A, Khan MS. Antimalarials. 13. 5-Alkoxy analogues of 4-methylprimaquine. *J Med Chem*. 1982 Aug;25(8):964–8.
- [24] Eswaran S, Adhikari AV, Shetty NS. Synthesis and antimicrobial activities of novel quinoline derivatives carrying 1,2,4-triazole moiety. *Eur J Med Chem*. 2009 Nov;44(11):4637–47, <https://linkinghub.elsevier.com/retrieve/pii/S0223523409003602>. [cited 2022 Dec 4].
- [25] Zhang SS, Tan QW, Guan LP. Antioxidant, anti-inflammatory, antibacterial, and analgesic activities and mechanisms of quinolines, indoles and related derivatives. *Mini Rev Med Chem*. 2021;21(16):2261–75.
- [26] Kara M, Assouguem A, Fadili ME, Benmessaoud S, Alshawwa SZ, Kamaly OA, et al. Contribution to the Evaluation of physicochemical properties, total phenolic content, antioxidant potential, and antimicrobial activity of vinegar commercialized in Morocco. *Molecules*. 2022 Jan;27(3):770, <https://www.mdpi.com/1420-3049/27/3/770>. [cited 2022 Mar 13].
- [27] Wilson WD, Zhao M, Patterson SE, Wydra RL, Janda L, Strekowski L, et al. ChemInform abstract: design of RNA interactive Anti-HIV-1 agents: unfused aromatic intercalators. *ChemInform*. 1992 Nov;23(44):311. doi: 10.1002/chin.199244311 [cited 2022 Dec 5].
- [28] Maguire MP, Sheets KR, McVety K, Spada AP, Zilberstein A. A new series of PDGF receptor tyrosine kinase inhibitors: 3-substituted quinoline derivatives. *J Med Chem*. 1994 Jul;37(14):2129–37.
- [29] El-Mernissi R, El Khatibi K, Khaldan A, Bouamrane S, El Mchichi L, Mohammed Aziz A, et al. Designing of novel quinolines derivatives

- as hepatocellular carcinoma inhibitors by using in silico approaches. *Biointerface Res Appl Chem*. 2022;13(3):1–15.
- [30] Khaldan A, Bouamrane S, El-mernissi R, Ouabane M, Alaqrbeh M, Maghat H, et al. Design of new α -glucosidase inhibitors through a combination of 3D-QSAR, ADMET screening, molecular docking, molecular dynamics simulations and quantum studies. *Arab J Chem*. 2024 Mar;17(3):105656, <https://linkinghub.elsevier.com/retrieve/pii/S1878535224000583>. [cited 2024 Mar 6].
- [31] Sybyl-X. Molecular modeling software packages. USA: Inc St Louis MO; 2012. <http://www.tripos.com>.
- [32] Clark M, Cramer RD, Van Opdenbosch N. Validation of the general purpose tripos 5.2 force field. *J Comput Chem*. 1989 Dec;10(8):982–1012. doi: 10.1002/jcc.540100804 [cited 2021 Jan 30].
- [33] El-Mernissi R, Khaldan A, Bouamrane S, Rehman HM, Alaqrbeh M, Ajana MA, et al. 3D-QSAR, molecular docking, simulation dynamic and ADMET studies on new quinolines derivatives against colorectal carcinoma activity. *J Biomol Struct Dyn*. 2024;42(7):3682–99. doi: 10.1080/07391102.2023.2214233.
- [34] Hamza S, Abid A, Khanum A, Chohan TA, Saleem H, Maqbool Khan K, et al. 3D-QSAR, docking and molecular dynamics simulations of novel Pyrazolo-pyridazinone derivatives as covalent inhibitors of FGFR1: a scientific approach for possible anticancer agents. *J Biomol Struct Dyn*. 2024 Mar;42(5):2242–56. doi: 10.1080/07391102.2023.2212306 [cited 2024 Apr 19].
- [35] Raza A, Chohan TA, Sarfraz M, Chohan TA, Imran Sajid M, Tiwari RK, et al. Molecular modeling of pyrrolo-pyrimidine based analogs as potential FGFR1 inhibitors: a scientific approach for therapeutic drugs. *J Biomol Struct Dyn*. 2023 Dec;41(23):14358–71. doi: 10.1080/07391102.2023.2187638 [cited 2024 Apr 19].
- [36] Klebe G, Abraham U, Mietzner T. Molecular similarity indices in a comparative analysis (coMSIA) of drug molecules to correlate and predict their biological activity. *J Med Chem*. 1994 Nov;37(24):4130–46. doi: 10.1021/jm00050a010 [cited 2021 Feb 26].
- [37] Wang F, Yang W, Zhou B. Studies on the antibacterial activities and molecular mechanism of GyrB inhibitors by 3D-QSAR, molecular docking and molecular dynamics simulation. *Arab J Chem*. 2022 Jun;15(6):103872, <https://linkinghub.elsevier.com/retrieve/pii/S1878535222001885>. [cited 2024 Mar 6].
- [38] EL-Mernissi R, Khatabi EL, Khaldan K, El Mchichi A, Ajana L, Lakhlifi MA, T, et al. Design of new 3, 5-disubstituted indole as hematological anticancer agents using 3D-QSAR, molecular docking and drug-likeness studies. *Mater Today: Proc*. 2021;45:7608–14, <https://linkinghub.elsevier.com/retrieve/pii/S221478532102099X>. [cited 2021 Dec 31].
- [39] Golbraikh A, Tropsha A. Beware of q²! *J Mol Graph Model*. 2002;20(4):269–76, <https://linkinghub.elsevier.com/retrieve/pii/S1093326301001231>. [cited 2021 Dec 31].
- [40] Tropsha A, Gramatica P, Gombar VK. The importance of being earnest: validation is the absolute essential for successful application and interpretation of QSPR models. *QSAR Comb Sci*. 2003;22(1):69–77. doi: 10.1002/qsar.200390007 [cited 2021 Dec 25].
- [41] Baroni M, Clementi S, Cruciani G, Costantino G, Riganelli D, Oberrauch E. Predictive ability of regression models. Part II: Selection of the best predictive PLS model. *J Chemom*. 1992 Nov;6(6):347–56. doi: 10.1002/cem.1180060605 [cited 2021 Dec 25].
- [42] Rücker C, Rücker G, Meringer M. y-Randomization and its variants in QSPR/QSAR. *J Chem Inf Model*. 2007 Nov;47(6):2345–57. doi: 10.1021/ci700157b [cited 2021 Dec 25].
- [43] Mukhtar M, Saleem M, Nazir M, Riaz N, Shafiq N, Saleem H, et al. Identification of pyrrolizidine alkaloids and flavonoid glycosides through HR-LCMS/MS analysis, biological screening, DFT and molecular docking studies on *Heliotropium dasycarpum* Ledeb. *Arab J Chem*. 2023 May 1;16(5):104655, <https://www.sciencedirect.com/science/article/pii/S1878535223001168>. [cited 2024 Apr 19].
- [44] Salahub DR, Fournier R, Mlynarski P, Papai I, St-Amant A, Ushio J. Gaussian-based density functional methodology, software, and applications. In: Labanowski JK, Andzelm JW, editors. *Density functional methods in chemistry*. New York, NY: Springer; 1991. p. 77–100. doi: 10.1007/978-1-4612-3136-3_6 [cited 2022 Aug 9].
- [45] Becke AD. Density-functional exchange-energy approximation with correct asymptotic behavior. *Phys Rev A*. 1988 Sep;38(6):3098–100. doi: 10.1103/PhysRevA.38.3098 [cited 2023 Oct 21].
- [46] El-Mernissi R, El Khatabi K, Khaldan A, ElMchichi L, Shahinozzaman M, Ajana MA, et al. 2-Oxoquinoline arylaminothiazole derivatives in identifying novel potential anticancer agents by applying 3D-QSAR, docking, and molecular dynamics simulation studies. *J Mex Chem Soc*. 2021 Dec;66(1):79–94. <https://www.jmcs.org.mx/index.php/jmcs/article/view/1578>. [cited 2022 Feb 12].
- [47] Parr RG, Pearson RG. Absolute hardness: companion parameter to absolute electronegativity. *J Am Chem Soc*. 1983 Dec;105(26):7512–6. doi: 10.1021/ja00364a005. [cited 2023 Feb 3].
- [48] Agwamba EC, Udoikono AD, Louis H, Udo EU, Benjamin I, Igbalagh AT, et al. Synthesis, characterization, DFT studies, and molecular modeling of azo dye derivatives as potential candidate for trypanosomiasis treatment. *Chem Phys Impact*. 2022 Jun;4:100076, <https://www.sciencedirect.com/science/article/pii/S2667022422000159>. [cited 2023 Feb 5].
- [49] Parr RG, Szentpály LV, Liu S. Electrophilicity index. *J Am Chem Soc*. 1999 Mar;121(9):1922–4. doi: 10.1021/ja983494x [cited 2023 Feb 5].
- [50] Yousef TA, Alhamzani AG, Abou-Krishna MM, Kanthimathi G, Raghu MS, Kumar KY, et al. Synthesis, molecular docking study and anticancer activity of novel 1,3,4-oxadiazole derivatives as potential tubulin inhibitors. *Heliyon*. 2023 Feb;9(2):e13460, <https://www.sciencedirect.com/science/article/pii/S2405844023006679>. [cited 2024 Apr 26].
- [51] Federico LB, Silva GM, Gomes SQ, Francischini IAG, Barcelos MP, dos Santos CBR, et al. Potential colchicine binding site inhibitors unraveled by virtual screening, molecular dynamics and MM/PBSA. *Comput Biol Med*. 2021 Oct 1;137:104817, <https://www.sciencedirect.com/science/article/pii/S0010482521006119>. [cited 2024 Apr 26].
- [52] Systèmes D. Free download: BIOVIA Discovery Studio Visualizer. Dassault Systèmes; 2020. <https://discover.3ds.com/discovery-studio-visualizer-download> [cited 2022 Dec 31].
- [53] DeLano W, Bird PA, Wright C. A double blind study of antrafenine, naproxen and placebo in osteoarthritis. USA: Pymol; 2017. <http://www.pymol.org>.
- [54] Al-Qadisy I, Saeed WS, Al-Odayni AB, Alrabie A, Al-Faqeeh LAS, Al-Adhrai A, et al.. Antidiabetic, antioxidant and cytotoxicity activities of *ortho* - and *para* -substituted Schiff bases derived from metformin hydrochloride: Validation by molecular docking and *in silico* ADME studies. *Open Chem*. 2023 Sep;21(1):20230125. doi: 10.1515/chem-2023-0125/html [cited 2024 Mar 12].
- [55] El-Mernissi R, Khatabi KE, Khaldan A, Bouamrane S, Mchichi LE, Aziz M, et al. In silico studies of novel styrylquinoline derivatives as tubulin polymerization inhibitors against human ovarian carcinoma. *Malaysian J Biochem Mol Biol*. 2022;1:117–29. Special Issue.

- [56] Isvoran A, Ciorsac AA, Ostafe V. ADME-Tox profiling of some water soluble chitosan derivatives. *ADMET DMPK*. 2017 Sep;5(3):192–200. <http://pub.iapchem.org/ojs/index.php/admet/article/view/423> [cited 2023 Oct 21].
- [57] Batool A, Parveen S, Sha N, Salamatullah AM, Ibenmoussa S, Bourhia M. Computational study of ADME-Tox prediction of selected phytochemicals from *Punica granatum* peels. *Open Chem*. 2024;22(1):1–13.
- [58] Wan H. What ADME tests should be conducted for preclinical studies? *ADMET DMPK*. 2013 Aug;1(3):19–28. <http://pub.iapchem.org/ojs/index.php/admet/article/view/9>. [cited 2023 Oct 21].
- [59] Habib I, Chohan TA, Chohan TA, Batool F, Khurshid U, Khurshed A, et al. Integrated computational approaches for designing potent pyrimidine-based CDK9 inhibitors: 3D-QSAR, docking, and molecular dynamics simulations. *Comput Biol Chem*. 2024 Feb;108:108003, <https://www.sciencedirect.com/science/article/pii/S1476927123001949>. [cited 2024 Apr 19].
- [60] Pronk S, Páll S, Schulz R, Larsson P, Bjelkmar P, Apostolov R, et al. GROMACS 4.5: a high-throughput and highly parallel open source molecular simulation toolkit. *Bioinformatics*. 2013 Apr;29(7):845–54, <https://academic.oup.com/bioinformatics/article/29/7/845/253065>. [cited 2023 Oct 21].
- [61] Vanommeslaeghe K, Hatcher E, Acharya C, Kundu S, Zhong S, Shim J, et al. CHARMM general force field: A force field for drug-like molecules compatible with the CHARMM all-atom additive biological force fields. *J Comput Chem*. 2010 Mar;31(4):671–90. doi: 10.1002/jcc.21367 [cited 2023 Oct 21].
- [62] Krieger E, Nielsen JE, Spronk CAEM, Vriend G. Fast empirical pKa prediction by Ewald summation. *J Mol Graph Model*. 2006 Dec;25(4):481–6, <https://linkinghub.elsevier.com/retrieve/pii/S1093326306000477>. [cited 2023 Oct 21].
- [63] Wang XQ, Xia CL, Chen SB, Tan JH, Ou TM, Huang SL, et al. Design, synthesis, and biological evaluation of 2-arylethenylquinoline derivatives as multifunctional agents for the treatment of Alzheimer's disease. *Eur J Med Chem*. 2015 Jan 7;89:349–61.
- [64] Tunkel J, Mayo K, Austin C, Hickerson A, Howard P. Practical considerations on the use of predictive models for regulatory purposes. *Environ Sci Technol*. 2005 Apr;39(7):2188–99. doi: 10.1021/es049220t [cited 2024 Apr 27].
- [65] Netzeva TI, Worth AP, Aldenberg T, Benigni R, Cronin MTD, Gramatica P, et al. Current status of methods for defining the applicability domain of (quantitative) structure-activity relationships: the report and recommendations of ECVAM Workshop 52. *Altern Lab Anim*. 2005 Apr;33(2):155–73. doi: 10.1177/026119290503300209. [cited 2024 Apr 27].
- [66] Cherrate M, EL-Mernissi R, Bouymajane A, Filali FR, Trovato E, Echchgadda G, et al. Chemical composition, antioxidant/antibacterial activities and ADMET study of the essential oil isolated from the aerial parts of *Ziziphora hispanica* grown in Morocco. *J Essent Oil Res*. 2023;35(2):128–35. doi: 10.1080/10412905.2023.2170483 [cited 2023 Feb 1].
- [67] El-Mernissi R, Khatabi KE, Khaldan A, Bouamrane S, Ajana MA, Lakhliifi T, et al. New compounds based on 1H-pyrrolo[2,3-b]pyridine as potent TNIK inhibitors against colorectal cancer cells. *Molecular modeling studies. Moroccan J Chem*. 2023;11(01):20–33.